Low-lying states in ^{12}Be using one-neutron transfer reaction

J. Chen *et al.*

Phys. Rev. C **98**, 014616 — Published 24 July 2018

DOI: 10.1103/PhysRevC.98.014616

Study of the low-lying states in ^{12}Be using one neutron transfer reaction

J. Chen,[1,2] J. L. Lou,[1,*] Y. L. Ye,[1] Z. H. Li,[1] D. Y. Pang,[3] C. X. Yuan,[4] Y. C. Ge,[1] Q. T. Li,[1] H. Hua,[1] D. X. Jiang,[1] X. F. Yang,[1] F. R. Xu,[1] J. C. Pei,[1] J. Li,[1] W. Jiang,[1] Y. L. Sun,[1] H. L. Zang,[1] Y. Zhang,[1] G. Li,[1] N. Aoi,[5] E. Ideguchi,[5] H. J. Ong,[5] J. Lee,[6] J. Wu,[1,6] H. N. Liu,[1,6] C. Wen,[1,6] Y. Ayyad,[5] K. Hatanaka,[5] D. T. Tran,[5] T. Yamamoto,[5] M. Tanaka,[5] and T. Suzuki[5]

[1]*School of Physics and State Key Laboratory of Nuclear Physics and Technology, Peking University, Beijing 100871, China*
[2]*Physics Division, Argonne National Laboratory, Argonne, Illinois 60439, USA*
[3]*School of Physics and Nuclear Energy Engineering, Beijing Key Laboratory of Advanced Nuclear Materials and Physics, Beihang University, Beijing 100191, China*
[4]*Sino-French Institute of Nuclear Engineering and Technology, Sun Yat-Sen University, Zhuhai 519082, China*
[5]*Research Center for Nuclear Physics, Osaka University, Osaka, 567-0047, Japan*
[6]*RIKEN (Institute of Physical and Chemical Research), 2-1 Hirosawa, Wako, Saitama 351-0198, Japan*

(Dated: June 29, 2018)

A new one-neutron adding reaction on ^{11}Be was performed at 26.9A MeV. The elastic scattering data was measured simultaneously to determine the target component and optical potentials for the entrance channel. A special isomer-tagging method was used to determine the cross sections for the 0^+_2 state. Based on the ratio of the $s-$wave spectroscopic factors of the 0^+_1 and 0^+_2 states, along with the previously reported $p-$wave intensities, the $s-$ and $d-$wave components of these two states were obtained and compared with shell model calculations using various interactions. The result shows a dominant $d-$wave strength in the ground state of ^{12}Be, and reveals the dominance of sd- and sp-single-particle configurations in the 2^+ and 1^- state of ^{12}Be, respectively. Together with the configuration mixing analysis, the relative spectroscopic factors, which are shown to be less sensitive to the different choice of optical potentials, provide important insights on the wave functions for the low-lying states of ^{12}Be.

I. INTRODUCTION

In the well-established nuclear shell model, nucleons are assumed to arrange themselves into the single-particle orbitals, which group into shells according to the magic numbers. The conventional shell model and magic numbers are obtained by solving the Schrödinger equation in a mean field potential. In the light nuclei region, especially approaching the neutron or proton drip line, many factors could contribute to the change or disappearance of the conventional shells, such as the monopole interaction between proton and neutron [1], the weak binding of the nucleons approaching the drip line [2–4], and the three-body force in nuclei [5]. As a well-recognized example, the ground state $(1/2^+)$ and the first excited state $(1/2^-)$ of the halo nucleus ^{11}Be are inverted with respect to the predictions from conventional independent particle shell model. For its ground state (g.s.), numerous measurements have demonstrated a dominant (60% $\sim$ 80%) configuration of ^{10}Be+$n(2s_{1/2})$ [6, 7]. The present work focuses on its neighbouring nucleus ^{12}Be at the neutron-rich side, whose exotic structures were observed in various measurements.

The excitation energies of the 2^+_1 (2.107 MeV), 0^+_2 (2.251 MeV) and 1^-_1 (2.710 MeV) states in ^{12}Be are much lower than other $N = 8$ nuclei, like ^{14}C and ^{16}O, indicating the reduction of the $N = 8$ shell in ^{12}Be. This gives rise to many exotic phenomena of the ^{12}Be nucleus, such as the enhanced E1 transition from the ground state (0^+_1) to the 1^-_1 state [8], the large quadruple transition strength from the 2^+_1 state to 0^+_1 g.s. [9, 10], and the strong sd-intruder configuration in the 0^+_1 (g.s.) of ^{12}Be. Recent experimental work has extensively taken place, demonstrating the intruder configuration in the 0^+_1 (g.s.) of ^{12}Be, such as the knockout reactions [11, 12] and the charge-exchange reaction [13]. The p-, s- and d-wave spectroscopic factors (SFs) of the ^{12}Be 0^+_1 ground state were investigated by the knockout reactions [11, 12]. After normalizing the sum of the SFs to the occupation number, the result was compared to theoretical calculations in the first row of Table I. The p-wave intensities for the first two 0^+ states, which were obtained from the charge-exchange reaction [13], are shown in the second row of Table I.

Many theoretical studies have been performed to explore the configuration of the low-lying states in ^{12}Be, including the shell model calculations by Barker [14] and Fortune *et al.* [15], the three-body model predictions by Nunes *et al.* [16] and Redondo *et al.* [17], the nuclear field theory approach by Gori *et al.* [18], and the random-phase approximation (RPA) [19]. The intensity of each component in the low-lying states is summarized in the lower panel of Table I. The individual intensity of the two lowest 0^+ states varies largely from case to case, especially for the 0^+_1 (g.s.). The p-, s-, d-wave components contribute uniformly in Baker's wave function, while Fortune's and the three-body calculations predicted more than 50% s-wave component. The three-body calculation with the excitation of ^{10}Be core and the

* jllou@pku.edu.cn

TABLE I. Intensities of the $s(\alpha)$-, $d(\beta)$- and $p(\gamma)$-wave in the first two 0^+ states of ^{12}Be, from different measurements (upper panel), together with the results predicted by various theoritical calculations (lower panel).

0_1^+			0_2^+			
α_1(%)	β_1(%)	γ_1(%)	α_2(%)	β_2(%)	γ_2(%)	Ref
33[a]	38[a]	29[a]				[11, 12]
		24±5[b]			59±5[b]	[13]
19±7	57±7		39±2	2±2		this work
33	29	38	67	10	23	[14]
53	15	32	25	7	68	[15, 21]
31	42	27				[12, 16]
67∼76	10∼13	13∼19	15∼23	6∼8	71∼78	[17]
23	48	29				[18]
25[c]	21[c]	54[c]	62[c]	0[c]	38[c]	[19]

a using SFs of 0.42, 0.48 and 0.37 for s-, d- and p-components [11, 12, 22], respectively, which are normalized to give the intensities [21].
b p-wave intensities extracted from a charge-exchange experiment [13].
c from Table.2 and Table.3 of Ref. [19].

nuclear field theory approach supported relatively larger d-wave components, and the RPA calculation suggested a dominant p-wave component. The calculated ratio of different components depends sensitively on the core-nucleon Hamiltonian and the nucleon-nucleon residual interaction [20].

For the 2^+ state, the three-body calculation [17] suggested 82% sd-component. The RPA calculation [19] also supports a predominant sd-single-particle configuration. However, both calculations could not reproduce the excitation energy of the 2^+ state and the excitation of ^{10}Be core has to be included in the calculation to obtain the proper excitation energies, as shown in Ref. [16]. For the 1^- state, most calculations support the dominance of the ps-single-particle configuration [16, 17, 19].

One neutron transfer reaction is a powerful and sensitive tool to selectively populate the single-particle structure of nuclei [23–25]. The ^{11}Be$(d,p)^{12}$Be transfer reactions were previously studied at $5A$ MeV [22] and $2.8A$ MeV [26]. However, in the former measurement, the 0_2^+ state was not resolved from the 2^+ state, and the events of 1^- state were close to the threshold, resulting in larger uncertainty for the SFs extraction. The latter measurement suffered from the relatively low beam energy, and the cross sections at small center-of-mass angles were not covered. As a result, it does not allow a unique extraction of the SFs. Furthermore, without a reasonable normalization of the experimental SFs, it is not convenient to compare the SFs with theoretical calculations or other measurements. The present measurement of the ^{11}Be(d,p) at $26.9A$ MeV was specially designed to clarify these ambiguities.

Following the previous letter [27], we present here the details associated with the newly performed transfer reaction experiment to investigate the configuration of the low-lying states in ^{12}Be. In addition to the first two 0^+ states, which are the focus of the earlier work, the results for the 2^+ and 1^- states are reported here. Some $\ell = 2$ and $\ell = 0$ strengths in ^{12}Be were found to be missing, which are presumably in unbound states and likely in a third unseen 0^+ state, respectively. Furthermore, a reasonably consistent shell model description of the ^{11}Be and ^{12}Be is reported, although there are some remaining difficulties in reproducing properties of the 1^- state. Especially, the application of the isomer-tagging method and the sensitivity of the relative spectroscopic factors using various optical potentials were discussed in detail, as these are key factors for the conclusions of the present work. After normalization, the SFs of the low-lying states from the ^{11}Be(d,p) reaction at $26.9A$ MeV are reported and comparison are made with different theoretical calculations. In Section II, details for the experimental setup together with elastic scattering and one-neutron transfer cross sections are presented. In Section III, the SF for each state in ^{12}Be populated by the ^{11}Be(d,p) transfer reaction is extracted and comparisons are made with theoretical calculations. Detailed analysis and discussions associated with the isomer tagging method, quenching factors, relative SFs, single-particle strength and shell model calculations are presented here. A brief summary is given in the last section.

II. EXPERIMENT

The experiment was carried out at the exotic nuclei (EN) beam line, RCNP (Research Center for Nuclear Physics), Osaka University [28]. A ^{11}Be secondary beam at $26.9A$ MeV was produced with an intensity of 10^4 particles per second (pps) and a purity of about 95%. The secondary beam carried a 5% contamination of ^{9}Li, which was identified by the energy deposit and time of flight information from the beam line plastic scintillator. The momentum spread was reduced to around $\Delta P/P \leq 1\%$ to limit the energy resolution. Two parallel-plate avalanche counters (PPAC) placed upstream of the target provided beam tracking information, with the resolution of incident angles and hitting positions on the target less than 0.3° and 2.0 mm, respectively. Elastic scattering of ^{11}Be from protons or deuterons was measured by using a $(CH_2)_n$ (4.00 mg/cm^2) or a $(CD_2)_n$ (4.00 mg/cm^2) target, respectively, with the C-target (12.58 mg/cm^2) providing the background subtraction [29, 30]. The same $(CD_2)_n$ target was used for the ^{11}Be$(d,p)^{12}$Be reaction. All targets were tilted 15° to limit the energy loss of the recoiling light particles from the elastic or inelastic scattering channels.

The setup of detectors in this experiment is schematically shown in Fig. 1. A set of annular silicon detectors

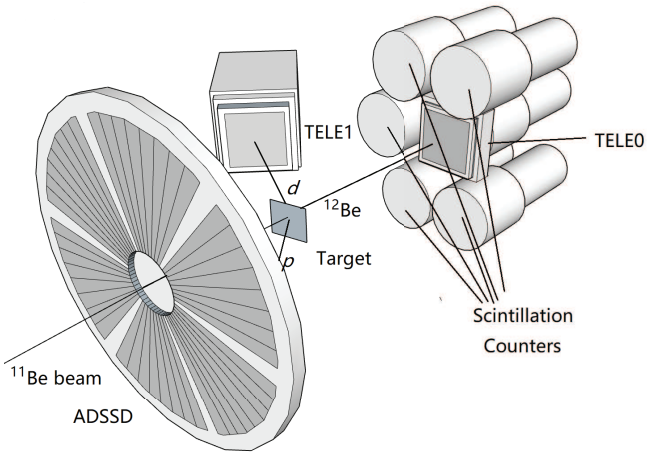

FIG. 1. Schematic sketch of the experimental setup for the present measurement.

(ADSSD) was installed at a distance of 135 mm upstream the target to detect the protons from the ^{11}Be$(d,p)^{12}$Be reaction, covering laboratory angles of 165°-135° relative to the beam direction. The ADSSD was composed of six sectors, each divided into sixteen 6.4-mm-wide rings on one side and eight wedge-shaped regions on the other side. The inner and outer radii are 32.5 mm and 135 mm, respectively. Two charged particle telescopes, TELE0 and TELE1, were placed 200 and 170 mm from the target to detect and distinguish the Be isotopes around 0° and the scattered protons/deuterons, respectively. The on-axis zero-degree telescope, TELE0, was consist of a double-sided silicon strip detector (DSSD) (1000 μm) and two large surface silicon detectors (SSDs) (1500 μm). The TELE1 was placed around 76° with respect to the beam direction, which was composed of a 300-μm DSSD, a 1500-μm SSD, and a layer of four CsI(Tl) crystals read out by photodiodes. Each DSSD is divided into 32 strips on both sides and has an active area of 62.5×62.5 mm^2. Taken into account the position resolution resulting from the PPACs, the overall angular resolutions of TELE1 and ADSSD were approximately 0.8° (FWHM) and 2.7° (FWHM), respectively. With the standard ΔE-E method, the silicon detectors could discriminate the isotopes lighter than carbon. A 1.0-MeV threshold was set for the scattered protons and deuterons to cut down the noise. Six scintillation counters surrounding the TELE0 were used to detect the γ-rays decaying from the isomeric state of ^{12}Be stopped in the TELE0.

The experiment was performed in inverse kinematics, in which discrimination of various reaction channels was achieved by a coincidence between the target-like particles (protons or deuterons) and the projectile-like fragments (Be isotopes). Data acquisition was performed using the software package babirlDAQ [31].

A. Elastic scattering reaction

In order to obtain the optical potential (OP) parameters for the entrance channel of the ^{11}Be(d,p) reaction, and also to deduce the proton component in the target, the elastic scattering data of ^{11}Be+p and ^{11}Be+d were collected during the experiment. Only the elastic scattering data are shown here, and the data from breakup channels were detailed in Refs. [29, 30]. The elastic scattering or breakup reaction channels were separated by the coincidence of ^{11}Be or ^{10}Be measured by the TELE0 and light particles (protons/deuterons) detected by the TELE1.

The present $(CD_2)_n$ target has larger thickness compared with those used in the previous experiments [22, 26], because of the different beam energies. The areal density (thickness) of the $(CH_2)_n$ or $(CD_2)_n$ target was determined by its weight and size, with very high precision (about 0.25% uncertainty depending on the applied apparatus). The $(CD_2)_n$ target is usually contaminated by the $(CH_2)_n$ impurity. By using the elastic scattering of ^{11}Be on both the $(CD_2)_n$ and the $(CH_2)_n$ targets and by detecting the well identified recoil protons, the H component in the $(CD_2)_n$ target relative to that in the $(CH_2)_n$ target was determined to be around 9.5%, by a precision of 0.6% (statistical error) [30]. In addition, a systematic error of 1.2% is estimated from the cuts applied in the data analysis processes. The non-uniformity of the target thickness is about 1.25% (0.05 mg/cm^2 non-uniformity relative to 4.00 mg/cm^2 total thickness). The overall uncertainty of the deuteron-target thickness is about 2%.

The angular distributions of ^{11}Be elastic scattering on protons and deuterons (as a ratio to the Rutherford cross sections) are presented in Fig. 2(a) and 2(b), respectively, with each data point corresponding to a laboratory angular width of 1.5°. Because most of the global OPs are mainly extracted from the stable nuclei data, renormalization factors for the real and imaginary central potentials are often required when applied to the scattering of light exotic nuclei [32, 33]. For the elastic scattering of ^{11}Be on protons, OP parameters were searched based on the CH89 [34] global OPs, and the resulting renormalization factors for the real and imaginary part are 0.78 and 1.02, respectively [29].

A new global deuteron potential, called DA1p [35], was recently developed, based on the experimental data of deuteron elastic scattering from $1p-$shell nuclei with incident energies between 5.25 and 170 MeV. This global potential is employed to calculate the elastic scattering cross sections of ^{11}Be on deuterons, which gives a reasonably well description of the present experimental cross sections in Fig. 2(b). Further investigation of the ^{11}Be+d elastic scattering cross sections including the core excitation in ^{11}Be or using the four-body model could be found in Refs. [30, 36]

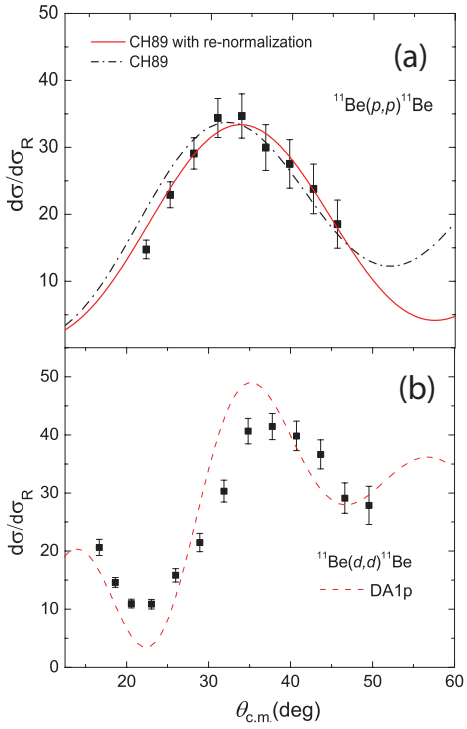

FIG. 2. The elastic scattering differential cross sections of ^{11}Be+p (a) and ^{11}Be+d (b) at 26.9A MeV. The data points have been divided by the Rutherford scattering cross sections. The black dash-dotted line in (a) donates the calculation result using the CH89 potential, while the red solid line is the result after application of the renormalization parameters (see details in the text). The red dashed line in (b) represents the calculation using the optical model with the DA1p potential.

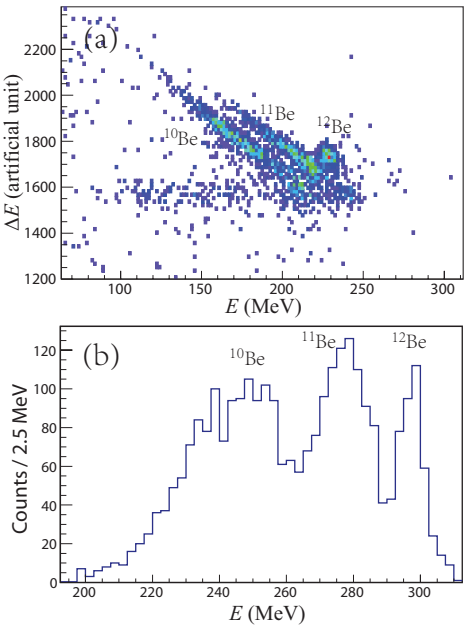

FIG. 3. (a) The PID in coincidence with the protons detected by the ADSSD. (b) Summed energy spectrum of the protons in ADSSD and the corresponding Be isotopes in TELE0. From high to low energies, three peaks mostly correspond to the ^{12}Be, ^{11}Be and ^{10}Be events in (a).

B. (d,p) transfer reaction

A particle identification (PID) spectrum, taken by the TELE0 and gated on the protons in the ADSSD, is shown in Fig. 3(a). The beam particles and other background were rejected by the timing coincidence between the protons and the projectile-like Be isotopes. The background from the C-target has been subtracted. It is worth noting that there are no events corresponding to ^{12}Be generated in the Carbon target run. ^{12}Be in the Fig. 3(a) must come from the (d,p) transfer reaction, while ^{11}Be and ^{10}Be, with the much broader energy spread, are most likely from one- or two-neutron decay following the population of ^{12}Be unbound states. This assumption was checked by the spectrum displayed in Fig. 3(b). It shows the sum of the proton energy in the ADSSD and the total energy of Be isotopes in TELE0, which should be equal to the beam energy if every fragment was detected. The events in the three peaks correspond to the population of bound states in ^{12}Be, unbound states decaying to ^{11}Be+n and ^{10}Be+2n, respectively. The energy difference between two adjacent peaks is around 27 MeV, corresponding to the average energy of one escaping neutron.

Gated on ^{12}Be in Fig. 3(a), the kinematics of the protons detected in the ADSSD are shown in Fig. 4(a) based on the detected energies and angles. The excitation energy in ^{12}Be was deduced accordingly, as shown in Fig. 4(b). The events corresponding to the 0_1^+ ground state are free from the detection loss or background owing to the relatively higher proton energies. Monte Carlo simulations give an energy resolution of about 1.1 MeV (FWHM), in agreement with the width of the 0_1^+ (g.s.) peak in Fig. 4(b). A large broad peak was contributed by the events belonging to the 2.107-, 2.251- and 2.710-MeV states in ^{12}Be.

The isomer-tagging method was used to discriminate the 0_2^+ state. The 0_2^+ state is well-known as an isomeric state with a life-time of 331 ± 12 ns [37] and an E0-decay (via e^+e^- pair creation) branching ratio of $83 \pm 2\%$ [38]. The ^{12}Be ions in the 0_2^+ isomeric state were stopped in the TELE0 and the 0.511-MeV γ-rays from the e^+e^- annihilations were measured by the six scintillation detectors surrounding the TELE0 (see Fig. 1). This kind of decay-tagging method has been successfully applied in many particle-emission experiments [39–41]. The ^{12}Be, protons and γ-rays triple-timing-coincidence within 3 μs was required to obtain the events belonging to the decay from the 0_2^+ state. The energy spectrum of the γ-ray within the triple-coincidence is presented in Fig. 4(c), where the significance of the 0.511-MeV γ-ray peak is clear. The time spectrum of these 0.511-MeV γ-ray was

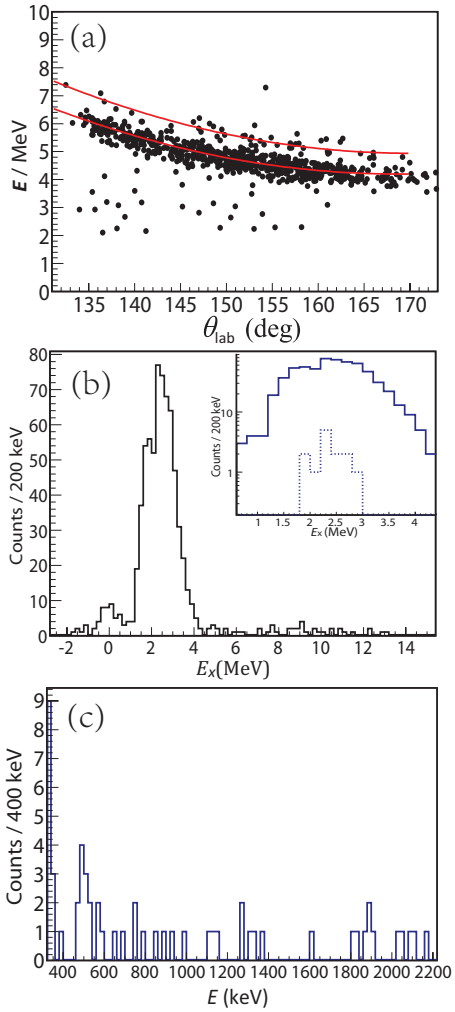

FIG. 4. (a) The measured proton energies versus the laboratory angles, gated on the ^{12}Be in the TELE0. The red solid lines illustrate the calculated kinematics of the ^{11}Be(d,p) transfer reaction to the 0^+_1 (g.s.) and the 2.251-MeV excited state. (b) The excitation energy spectrum of ^{12}Be deduced using the protons in (a). The dotted curve in the inset shows the events in coincidence with the 0.511-MeV γ-rays detected by the scintillation counters. (c) The γ-ray energy spectrum in coincidence with ^{12}Be+p events within the 3 μs time window.

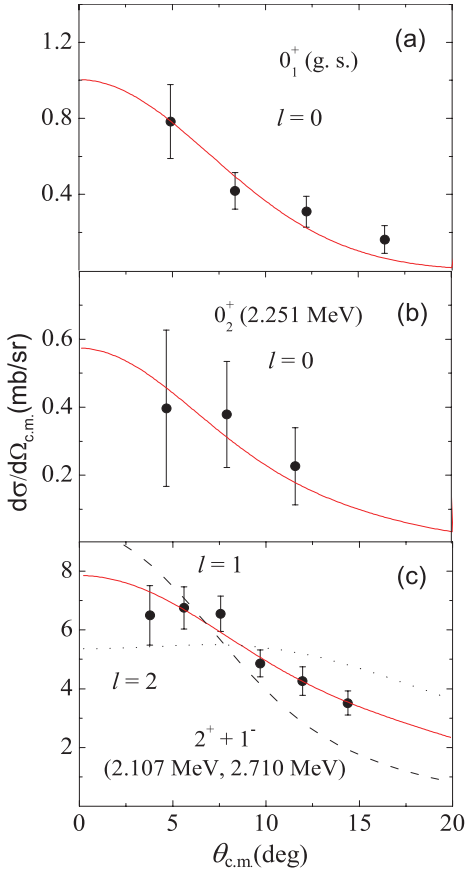

FIG. 5. Measured differential cross sections of the ^{11}Be$(d,p)^{12}$Be reaction at 26.9A MeV (solid dots), together with the FR-ADWA calculations normalized using the SFs, for (a) the ground state (0^+_1), (b) the isomeric state (0^+_2), and (c) the summed 2^+ and 1^- states. ℓ in each figure stands for the transferred orbital angular momentum.

fitted by an exponential decay curve. The extracted half-life time is 270 $\pm$ 120 ns, in agreement with the reported value [37]. The detection efficiency for the 0.511-MeV γ-rays, generated from the e^+e^- annihilation, was estimated to be 23$\pm$1% using the GEANT4 code [42], considering the realistic experimental setup.

The random or accidental coincident backgrounds were checked carefully. Firstly we selected the ^{11}Be and protons coincident event-sample with the same number of events as for ^{12}Be coincided with protons, and checked the simultaneously observed 0.511-MeV γ-rays. For each of the possible event-samples (there are much more events for ^{11}Be+p than for ^{12}Be+p), we found only 0 or 1 event having the 0.511-MeV γ-ray coincidence, to be compared to 14 events for the ^{12}Be+$p+\gamma$ coincidence. In addition, the timing of the former γ-ray (if any) appears always at 0 ns. The similar check was also performed for other possible coincidences. It is evident that the observed 0.511-MeV γ-rays within the ^{12}Be+$p+\gamma$ coincidence are truly from the ^{12}Be+p system. Secondly we checked the empty-target or the carbon-target runs and find no ^{12}Be+$p+\gamma$ triple-coincidence events, confirming the expected reaction channel as the source of those observed triple-coincident events. The random coincident events were excluded for this triple-coincidence considering the low coincident rate and the relatively narrow time window.

Although the contaminations from the accidentally coincidence are negligible for the triple-coincidence events, the 2.107- and 2.710-MeV γ-rays decaying from the ^{12}Be excited states may still feed into the triple-coincidence time-window and create possible background. These

backgrounds can be analyzed quantitatively. Firstly, the branching-ratio of the 0.144 + 2.107-MeV γ-rays decay is only 17%, compared with 83% for the e^+e^- pair-decay, out of the total decay from the 2.251-MeV (0_2^+) isomeric state [38]. That is why we do not see the 2.107 MeV peak in Fig. 4(c) considering the total statistics. Furthermore, based on the detailed Monte Carlo simulations using the code GEANT4, the detection efficiency is $23 \pm 1\%$ for the 0.511-MeV γ-rays produced and directly emitted from the TELE0, but only about 0.2% for the 2.107-MeV γ-rays which lead to emission of 0.511-MeV γ-rays via the pair creations interactions with the detector material. Therefore, this unfavorable indirect contribution to the 0.511- MeV γ-ray-spectrum can be ignored. Other indirect sources might be the prompt excitation and decay of the 2.710-MeV (1^-) and 2.107-MeV (2^+) states in ^{12}Be. However, since these γ-rays are emitted from the target, not from the TELE0, their indirect contribution to the 0.511-MeV γ-rays spectrum is further reduced to less than 0.1%, based on the simulation. We also noticed that the 2.710-MeV (1^-) state has almost no decay-branching to the 2.251-MeV (0_2^+) isomeric state, due to the energy dependence of the γ-decay strength.

III. ANALYSIS OF THE EXPERIMENTAL RESULTS

A. Extraction of the SFs

Differential cross sections for the ^{11}Be(d,p) reaction to the ground state and excited states in ^{12}Be at 26.9A MeV are presented in Fig. 5. The events belonging to the ground state (low-lying excited states) are selected by a cut from -1.0 to 0.6 MeV (0.6 to 4.2 MeV) on the excitation energy spectrum (Fig. 4(b)). A gate between 0.4 and 0.6 MeV on the γ-ray energy spectrum (Fig. 4(c)) is applied to select the 0.511-MeV γ-ray decay from the isomeric 0_2^+ state. Especially, the events belonging to the isomeric state are selected by applying the coincidence between the proton, ^{12}Be and γ-ray. The summed cross sections of 2^+ and 1^- states are plotted in Fig. 5(c) with those for the 0_2^+ state subtracted. The error bars in Fig. 5 are statistical only. The systematic error is estimated to be less than $\sim$ 10%, taken into consideration the uncertainties in the detection efficiency determination($\sim$ 5%), the $(CD_2)_n$ target thickness ($\sim$ 2%), and the cuts on the PID spectrum ($\sim$ 4%) and the excitation energy spectrum ($\sim$ 5%).

To extract the SFs, theoretical calculations were carried out using approach of finite-range adiabatic distorted wave approximation (FR-ADWA), which includes explicitly the coupling effect of deuterons breakup [6]. In the present calculation using FRESCO [43], the $p+n$ potential is given by the Reid soft-core interaction [44]. The ^{11}Be+n binding potential is a Woods-Saxon form with a fixed radius and diffuseness parameter of 1.25 fm and 0.65 fm, respectively. The well depth of the binding potential was adjusted to reproduce the correct excitation energies. The entrance channel OP is obtained by folding the ^{11}Be+p and ^{11}Be+n potentials, with the former extracted from the present elastic-scattering data in Section II and the latter one from global potentials. Two renormalization factors ($\lambda_V = 0.78$ and $\lambda_W = 1.02$) were applied on the global potentials (CH89) as stated above. The exit channel OP is extracted from the data in Ref. [45].

The SFs of each state for the selected single-particle component, was extracted from the present data. The calculated cross sections, multiplied by the corresponding SFs are shown in Fig. 5. The $s-$wave single-particle components were selectively populated in the 0_1^+, 0_2^+ states, whose SFs were determined to be $0.20^{+0.03}_{-0.04}$ and $0.41^{+0.11}_{-0.11}$, respectively, as shown in Fig. 5(a) and (b). Considering the ground state of ^{11}Be being $1/2^+$, the single-particle components populated in the 2^+ or 1^- states should carry a very pure angular momentum of $\ell = 1$ or $\ell = 2$. Data in Fig. 5(c) for the mixed 2^+ and 1^- states were fitted by the weighted sum of $S_1 \cdot (^{11}\text{Be} \otimes n(1d_{5/2})) + S_2 \cdot (^{11}\text{Be} \otimes n(1p_{1/2}))$, where S_1 and S_2 are SFs for the $d-$ and $p-$wave neutrons in the low-lying 2^+ and 1^- states in ^{12}Be, respectively. The red solid curve in Fig. 5(c) shows the best fit with $S1 = 0.26 \pm 0.05$ and $S2 = 0.76 \pm 0.17$. All the error bars here correspond to a 68.3% confidence level. Fitted results of single d-wave with $SF = 0.5$ and p-wave with $SF = 1.4$ are also represented by the dotted and dashed curves in Fig. 5(c), respectively.

Compared with previous (d,p) transfer reactions [22, 26], without considering the normalization procedure, the SF of 2^+ state from the present measurement seems to be compatible with two out of four sets of results reported in Ref. [26] for various selections of OPs, namely 0.30 ± 0.10 (set II), and 0.40 ± 0.10 (set III). Besides, the SF of 1^- state here is in moderate agreement with the result of set IV. In order to compare quantitatively the present SF results with those from theoretical calculations and from other measurements, a normalization is required [46].

B. Quenching factor

The experimentally observed SFs are often smaller than the shell-model predictions, an effect being exhibited by a reduction or quenching factor. This quenching phenomenon was firmly established from $(e,e'p)$ knockout reactions [47, 48]. Using nuclear reactions, such as knockout or transfer reactions, this quenching effect is also generally confirmed. Since the individual SF_{exp} might be sensitive to the choice of OPs and the practical experimental conditions, the sum rule method was developed to define the relative SF using the quenching or normalization factor [49]. By definition

the quenching factor in nucleon-transfer reaction is [46]

$$F_q = \frac{1}{2j+1}[\Sigma(\frac{\sigma_{exp}}{\sigma_{DW}})_j^{add} + \Sigma(\frac{\sigma_{exp}}{\sigma_{DW}})_j^{rem}], \quad (1)$$

where the sum of the adding and removing relative cross sections for a given ℓ, j represents the total degeneracy of that orbit. For instance, Ref. [46] reported a consistent quenching factor of about 0.55 for a large number of nuclei, with a root-of-mean-square spread of 0.10.

Once the sum rule (SR) was established, the individual SF_{exp} can be normalized using the sum rule to give the intensity (percentage) of each component, which can be reasonably used to compare with the theoretical predictions. The SF normalization procedure does not change the ratio between the SFs. Furthermore, the ratio of these SFs is not very sensitive to the different selection of the OPs [24, 46] (see next subsection D). We will use this ratio in the following discussions to deduce the single-particle components.

Using the standard method proposed by Barker [14], the wave functions of the two low-lying 0^+ states can be written as $|0_i^+\rangle = a_i|1s_{1/2}^2\rangle + b_i|0d_{5/2}^2\rangle + c_i|0p_{1/2}^2\rangle (i = 1, 2)$, with the normalization relations $a_i^2 + b_i^2 + c_i^2 = \alpha_i + \beta_i + \gamma_i = 1$ and the orthogonal requirement $a_1 \cdot a_2 + b_1 \cdot b_2 + c_1 \cdot c_2 = 0$. From the present measurement, we have $\alpha_1/\alpha_2 = 0.20/0.41 = 0.49$. Using the previously measured $1p_{1/2}$-wave strengths in the charge-exchange reaction, the extracted values are $\gamma_1 = 0.24$ and $\gamma_2 = 0.59$ within the $p-sd$ model space. Combining all these conditions, the intensities were deduced: $\alpha_1 = 0.19 \pm 0.07, \beta_1 = 0.57 \pm 0.07, \gamma_1 = 0.24 \pm 0.05, \alpha_2 = 0.39 \pm 0.02, \beta_2 = 0.02 \pm 0.02, \gamma_2 = 0.59 \pm 0.05$ [27].

According to the experimental as well as the theoretical definition of the intensity (I) [14], which is the SF divided by the adopted sum rule and hence sums up to 100%, together with the expression of Ref. [13], the quenching factor can easily be deduced:

$$F_q = \frac{SF_{exp}}{I \cdot (2j+1)} \quad (2)$$

In our case $j = 1/2$. Using the $SF_{exp} = 0.20$ (or 0.41) obtained from the present potential and the intensity $\alpha_1 = 0.19$ (or $\alpha_2 = 0.39$), the quenching factor F_q can easily be deduced to be 0.53. This factor is quantitatively consistent with 0.55(0.10), which was obtained from the global analysis [46] and has been used to normalize the experimental SFs to compare with the theoretical calculations.

C. Single-particle strengths

The SFs after application of the quenching factor are defined as $SF = SF_{exp}/F_q$. Using the SFs for the 2^+ and 1^- state, their corresponding strengths can be determined by

$$GS = \frac{2J_f+1}{2J_i+1}SF, \quad (3)$$

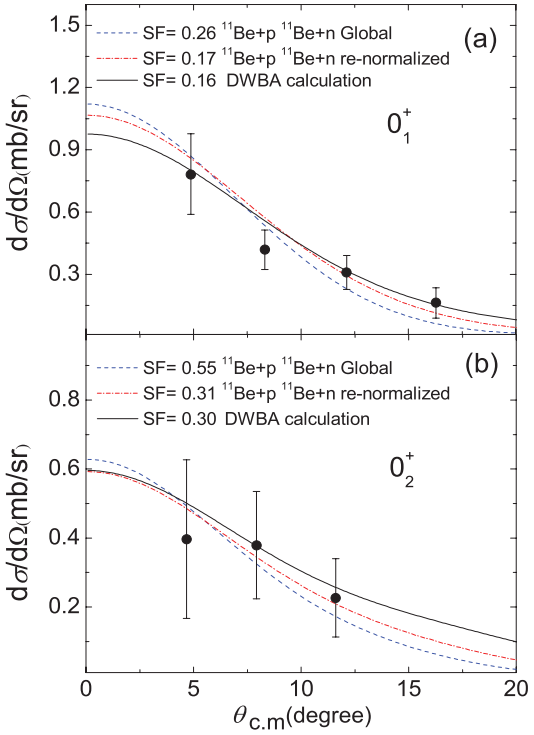

FIG. 6. The presently measured ^{11}Be$(d,p)^{12}$Be differential cross sections for the first (a) and second (b) 0^+ states together with calculations using different OPs. The calculations using the local or global potentials are fitted to the data to extract the respective SFs. See text for more details.

where $J_i = 1/2$ and J_f is the spin of the final states in ^{12}Be [24, 46]. According to the sum rule [46, 48], the $\ell = 0$, $\ell = 1$ and $\ell = 2$ single-particle strength should summed up to be the vacancies of the corresponding orbitals in ^{11}Be, which are ~ 1 ($2s_{1/2}$ orbital), ~ 2 ($1p_{1/2}$ orbital) and ~ 6 ($1d_{5/2}$ orbital), respectively. For the 0^+, 1^- and 2^+ states, their single-particle strength were determined to be 0.58 ± 0.15, 2.15 ± 0.48 and 1.23 ± 0.23, respectively. It is obvious that the 1^- state carries most of the single-particle strength while there is still some $\ell = 2$ strength missing, perhaps in some unbound states above the neutron separation energies. The third 0^+ state was predicted at about $E_x = 4.8$, $E_x = 5.5$ and $E_x = 8.5$ MeV, above $1n$- and $2n$-separation-energies of ^{12}Be, by H. T. Fortune [15], F.C. Barker [14, 21] and J. K. Smith [50] with shell model calculations, respectively, but was not observed in any experiment at or around these excitation energies. According to the analysis above, around a half of s-wave intensity was observed in the first two 0^+ states, and the rest half is expected in the unbound 0_3^+ state. In the future study, further search for the predicted 0_3^+ state is still anticipated.

TABLE II. Extracted SFs of 0_1^+ and 0_2^+ states corresponding to the calculations presented in Fig. 5 (Set1) and 6 (Set2-4).

	Optical potential	SF (0_1^+)	SF (0_2^+)	ratio
Set1	^{11}Be+p local, ^{11}Be+n global	0.20	0.41	2.05
Set2	^{11}Be+p local, ^{11}Be+n local	0.17	0.31	1.83
Set3	^{11}Be+p global, ^{11}Be+n global	0.26	0.55	2.11
Set4	^{11}Be+p global (DWBA)	0.16	0.30	1.88

D. Investigation using different OPs

We investigated the uncertainties of the SFs ratios caused by the OP selections. In Fig. 6 and Table II are presented the measured and the calculated cross sections, together with the extracted SFs, for the two low-lying 0^+ states. Here we used either the "local" or global potentials for both ^{11}Be+n and ^{11}Be+p systems. "local" here means the application of the renormalization factors to the depth of the global potentials, in order to better reproduce the elastic scattering data. Since no data for ^{11}Be+n scattering was available, we used the same renormalization factors as ^{11}Be+p for "local" ^{11}Be+n potential (see section II). The DWBA calculations using global DA1p optical model as the entrance channel OP are also presented here for comparison. From Table II it can be seen that, although the SFs may change about $\pm 21\%$ for 0_1^+ state or about $\pm 27\%$ for 0_2^+ state, the ratio of the SFs for the two states varies only about $\pm 7\%$. We applied this ratio in the present work due to its much better stability.

It should be noted that, for the halo nuclei, the application of the renormalization factors to the global potentials has been widely adopted [32]. Therefore, the systematic error of the SFs associated with the OPs should be less than the above demonstrated deviation of the SFs associated with "local" or global potentials. For the SFs of 2^+ and 1^-, different OPs as stated above have also been applied, resulting in around 18% uncertainty. Noted that there is around 7% uncertainty of the ratio α_1/α_2, there should also be a similar uncertainty for the quenching factor. It is much smaller than the uncertainties resulted from the statistics or the fitting procedure.

E. Shell model calculations

We have applied the shell model calculations, with the latest YSOX interaction [51, 52], to reproduce the experimentally observed SFs. The calculated individual $s-$, $d-$, and $p-$wave intensities for the low-lying bound states in ^{12}Be, represented by Case1, are compared to the ones from present measurement in Fig. 7. Although Case1 generally reproduced the individual intensities, it predicted an inverted energy-level order for 2^+ and 0_2^+ states. Furthermore, the $p-$wave intensity is a little higher than the experimental value [13], while the $d-$wave is lower than experiment. A decrease of 0.5 MeV for the $d-$orbit in the calculation would result in the correct level order, and also a better reproduction of the $p-$wave intensities was achieved, as displayed by Case2 in Fig. 7.

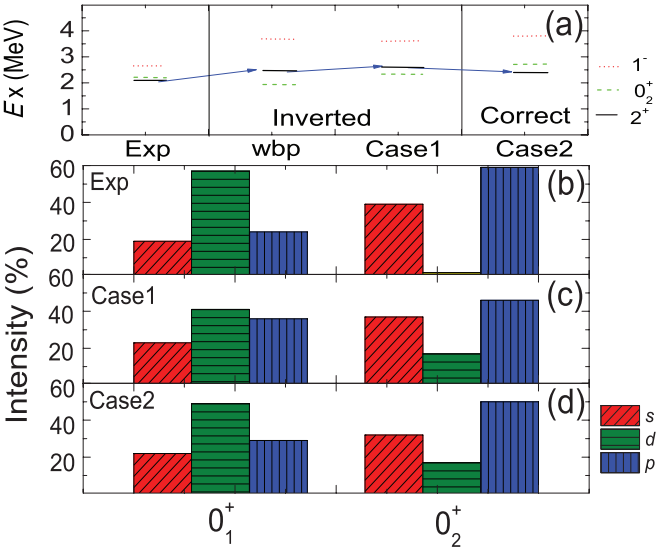

FIG. 7. (a) The level schemes of the low-lying states in ^{12}Be from the experimental data and shell model calculations with wbp [22] or YSOX Hamiltonian. The individual $s-$, $p-$ and $d-$wave intensities for the 0_1^+ and 0_2^+ states deduced from experiments (b) compared to those calculated using YSOX interaction in Case1 (c) and Case2 (d).

The SFs and configurations of the low-lying states of ^{12}Be calculated using the YSOX interaction (Case1), and those obtained after decreasing 0.5 MeV for the d-orbital (Case2) are shown in Table III. The experimental SFs were normalized using the quenching factor ($F_q = 0.53$). In the calculation, the ground state is dominated by the intruder configuration with two particles in the sd-shell, whereas the 0_2^+ has a much larger normal configuration (p-shell), in agreement with the experiments. The 1^- or 2^+ state is dominated by the configuration with one or two particles in the sd-shell, respectively.

The calculated SFs and excitation energies (E_x) of the 0_1^+, 2^+ and 0_2^+ states are in reasonable agreement with the experimental results, but those for the 1^- state show some deviations. Considering the ground state of ^{11}Be dominated by the s-wave component, the present SF of the 1^- or 2^+ state represents the sd- or sp-single-particle strength in the respective state. For the 2^+ state, the agreement of the experimental and calculated values supports the dominance of the sd-single-particle configuration in the calculation. The experimental SF for the 1^- state is higher than the calculated one, indicating higher sp-single-particle strength than the calculation. Generally, the YSOX interaction gives a very pure sd configuration for 2^+ and around 82% sp-single-

TABLE III. Experimental excitation energies and normalized SFs from present ^{11}Be(d,p) reactions, in comparison to the calculated values, together with the calculated $0-3\hbar\omega$ configurations of the low-lying states in ^{12}Be. The $0,1,2,3\hbar\omega$ represent the configurations where $0,1,2,3$ particles are excited to the sd-shell. Here Case1 and Case2 stands for the calculation results using YSOX and modified YSOX interactions, respectively. See text for more details.

J_π	$E_x(exp)$	$SF(exp)$	$E_x(theory)$	$SF(theory)$	$0\hbar\omega$	$2\hbar\omega$	$1\hbar\omega$	$3\hbar\omega$
0_1^+(Case1)	0.00	0.38(8)	0.00	0.44	36%	64%		
2^+ (Case1)	2.11	0.49(9)	2.594	0.41	5%	95%		
0_2^+(Case1)	2.24	0.77(21)	2.380	0.67	46%	54%		
1^- (Case1)	2.71	1.43(32)	3.628	0.69			93%	7%
0_1^+(Case2)	0.00	0.38(8)	0.00	0.42	30%	70%		
2^+ (Case2)	2.11	0.49(9)	2.439	0.42	7%	93%		
0_2^+(Case2)	2.24	0.77(21)	2.639	0.59	50%	50%		
1^- (Case2)	2.71	1.43(32)	3.868	0.69			94%	6%

TABLE IV. Some physical observables of ^{11}Be and ^{12}Be from the experiments and from the present shell model calculation using the YSOX interaction in Case1. The effective charges is fixed to be $e_p = 1.26$ and $e_n = 0.21$ in the present calculation.

	^{12}Be					^{11}Be				
	B(E2)[a] (e^2fm^4)	B(E2)[b] (e^2fm^4)	B(E1)[c] (e^2fm^2)	S_n (MeV)	S_{2n} (MeV)	S_n (MeV)	J_π g.s.	s intensity g.s.	E_x of $1/2^-$ (MeV)	p intensity $1/2^-$
calculation	33.19	9.15	0.00097	2.73	2.14	-0.59	g.s.	78%	0.90	86%
experiment	$40 \pm 11 \pm 4$ [9]	7.0 ± 0.6 [37]	0.051 ± 0.013 [8]	3.171 [53]	3.672 [53]	0.502 [53]	g.s. [53]	71% [6]	0.32 [53]	62% [6]

a From 0_1^+ to 2^+.
b From 0_2^+ to 2^+.
c From 0_1^+ to 1^-.

particle configuration for 1^- state. Our result supports this single-particle configuration.

The B(E2), B(E1) value, one- and two-neutron-separation energy (S_n and S_{2n}) of ^{12}Be, the S_n, energy levels and configurations of ^{11}Be were also calculated using the YSOX interaction, and the results are shown in Table IV. The inversion of ground state and $1/2^-$ first excited state in ^{11}Be, as well as the intensities of the main configuration in these two states are reasonably reproduced. The calculated S_n of ^{12}Be is in reasonable agreement with experimental value, while either the S_n of ^{11}Be or the S_{2n} of ^{12}Be shows relatively larger deviation, indicating that binding energy of ^{10}Be might be not well reproduced using this interaction. The B(E2) value (0_1^+ to 2^+) is consistent with the experimental observation, with the value for the transition from 0_2^+ to 2^+ a little higher than the experiment. At the meanwhile, the B(E1) is very different from the measured value, in addition to the deviation in the SF and excitation energy of 1^- state from the experimental values, as stated above. This indicates that the theoretical model still demands further development to better describe these experimentally observed qualities. It was found that the application of Woods-Saxon potential increases largely the calculated E1 amplitude (a factor of 50 in B(E1) in some cases) compared to the one with harmonic-oscillator basis, possibly because of the larger extension of the radial wave function [54].

F. Discussion

In the present ^{11}Be(d,p) transfer measurement, the single-particle components of the ground state and the isomeric state have been determined and the result shows a clear $d-$wave predominance in the ground state of ^{12}Be. This is a very dramatic evolution of the intruder mechanism from ^{11}Be, whose ground state is dominated by the $s-$wave component. The most recent knockout reaction performed on a proton target also provided evidence for the dominance of the d-wave component in the ground state of ^{12}Be [55].

The parity inversion due to the lowering of the intruder $2s_{1/2}$ orbital crossing the normal $1p_{1/2}$ orbital in ^{11}Be leads to the well-established one-neutron halo. The dominance of the d-wave component in ^{12}Be ground state is a possibly result of stronger pairing interaction that favors neutrons in higher ℓ orbital and hinders the halo formation [56]. From the microscopic view, the lowering of $1d_{5/2}$ orbital energy is related to the deformation of the nuclei, as shown in the Nilsson model. The enhanced collectivity of ^{12}Be was indicated in the electromagnetic quadruple transition measurement [9, 10]. This deformation might be related to the well-established $\alpha-$cluster

structures in the Be-isotope chain [57–61].

IV. SUMMARY

In summary, a new ^{11}Be$(d,p)^{12}$Be one neutron transfer reaction was carried out in inverse kinematics at 26.9A MeV. The experiment was specially designed to determine the thickness of the $(CD_2)_n$ target and to measure the cross sections of the 0^+_2 state. In order to obtain the $(CH_2)_n$ component in the $(CD_2)_n$ target and also to extract the OPs for the entrance channel, the elastic scattering cross sections of ^{11}Be+p and ^{11}Be+d were measured during the experiment. The possible background in the isomer-tagging method, which was used to determined the cross section of the 0^+_2 state, was analyzed in detail. The SFs of the low-lying states of ^{12}Be were extracted by comparing the experimental differential cross sections to the calculations using the FR-ADWA approach. The ratio of the SFs for the first two 0^+ states, along with the previously determined $p-$wave components were used to determine the single-particle components in the 0^+_1 and 0^+_2 states as well as the quenching factor. The relative spectroscopic factors were shown to be less sensitive to the different selection of optical potentials, and its application with the configuration mixing analysis provided important insights on the wave function of the 0^+_1 and 0^+_2 states. After application of the quenching factors on the experimental SFs, comparison was made directly with various shell-model calculations using the recently developed YSOX interaction. This interaction was found to reproduce reasonably various characteristics in ^{11}Be and ^{12}Be, while some improvement is still anticipated in the future. The $d-$wave component was shown to be dominant in the ground state of ^{12}Be. The dramatic configuration change from ^{11}Be(g.s.) to ^{12}Be(g.s.) might be attributed to the pairing interaction of the valence neutrons and the enhanced collectivity in the low-lying states of ^{12}Be. The present SFs for the 2^+ and 1^- state support dominance of sd- and sp-single-particle configuration , respectively. There might be some missing $\ell = 0$ and $\ell = 2$ strength in the unbound state of ^{12}Be, expecting to be explored by the future experiments.

ACKNOWLEDGMENTS

We thank the RCNP accelerator group and operators for providing the ^{13}C primary beam, and the technical staff of EN-course for the assistance. The authors from Peking University acknowledge the local support. This work is supported by the National Key R&D Program of China (Contract No: 2018YFA0404403), the National Natural Science Foundation of China (Nos. 11775004, 11775013, 11775316, 11535004, 11375017, and 11405005). D. T. T. and C. J. appreciate the support of the Nishimura International Scholarship Foundation and RCNP Visiting Young Scientist Support Program, respectively. J. C. acknowledges partial support by the FRIB-CSC Fellowship under Grand No.201600090345 and U.S. Department of Energy, Office of Science, Office of Nuclear Physics, under Contract No. DE-AC02-06CH11357 (ANL).

[1] T. Otsuka, R. Fujimoto, Y. Utsuno, B. A. Brown, M. Honma, and T. Mizusaki, Phys. Rev. Lett. **87**, 082502 (2001).
[2] C. R. Hoffman, B. P. Kay, and J. P. Schiffer, Phys. Rev. C **89**, 061305 (2014).
[3] C. R. Hoffman, B. P. Kay, and J. P. Schiffer, Phys. Rev. C **94**, 024330 (2016).
[4] B. P. Kay, C. R. Hoffman, and A. O. Macchiavelli, Phys. Rev. Lett. **119**, 182502 (2017).
[5] T. Otsuka, T. Suzuki, J. D. Holt, A. Schwenk, and Y. Akaishi, Phys. Rev. Lett. **105**, 032501 (2010).
[6] K. T. Schmitt, K. L. Jones, A. Bey, S. H. Ahn, D. W. Bardayan, J. C. Blackmon, S. M. Brown, K. Y. Chae, K. A. Chipps, J. A. Cizewski, K. I. Hahn, J. J. Kolata, R. L. Kozub, J. F. Liang, C. Matei, M. Matoš, D. Matyas, B. Moazen, C. Nesaraja, F. M. Nunes, P. D. O'Malley, S. D. Pain, W. A. Peters, S. T. Pittman, A. Roberts, D. Shapira, J. F. Shriner, M. S. Smith, I. Spassova, D. W. Stracener, A. N. Villano, and G. L. Wilson, Phys. Rev. Lett. **108**, 192701 (2012).
[7] T. Aumann, A. Navin, D. P. Balamuth, D. Bazin, B. Blank, B. A. Brown, J. E. Bush, J. A. Caggiano, B. Davids, T. Glasmacher, V. Guimarães, P. G. Hansen, R. W. Ibbotson, D. Karnes, J. J. Kolata, V. Maddalena, B. Pritychenko, H. Scheit, B. M. Sherrill, and J. A. Tostevin, Phys. Rev. Lett. **84**, 35 (2000).
[8] H. Iwasaki, T. Motobayashi, H. Akiyoshi, Y. Ando, N. Fukuda, H. Fujiwara, Z. Flp, K. Hahn, Y. Higurashi, M. Hirai, I. Hisanaga, N. Iwasa, T. Kijima, A. Mengoni, T. Minemura, T. Nakamura, M. Notani, S. Ozawa, H. Sagawa, H. Sakurai, S. Shimoura, S. Takeuchi, T. Teranishi, Y. Yanagisawa, and M. Ishihara, Phys. Lett. B **491**, 8 (2000).
[9] N. Imai, N. Aoi, H. J. Ong, H. Sakurai, K. Demichi, H. Kawasaki, H. Baba, Z. Dombrdi, Z. Elekes, N. Fukuda, Z. Fulop, A. Gelberg, T. Gomi, H. Hasegawa, K. Ishikawa, M. Ishihara, H. Iwasaki, E. Kaneko, S. Kanno, T. Kishida, Y. Kondo, T. Kubo, K. Kurita, S. Michimasa, T. Minemura, M. Miura, T. Motobayashi, T. Nakamura, M. Notani, T. Ohnishi, A. Saito, S. Shimoura, T. Sugimoto, M. Suzuki, E. Takeshita, S. Takeuchi, M. Tamaki, H. Watanabe, and K. Yoneda, Phys. Lett. B **673**, 179 (2009).
[10] C. Morse, E. McCutchan, H. Iwasaki, C. Lister, V. Bader, D. Bazin, S. B. Novo, P. Chowdhury, A. Gade, T. Johnson, C. Loelius, E. Lunderberg, E. Merchan, V. Prasher, F. Recchia, A. Sonzogni, D. Weisshaar, and K. Whitmore, Phys. Lett. B **780**, 227 (2018).

[11] A. Navin, D. W. Anthony, T. Aumann, T. Baumann, D. Bazin, Y. Blumenfeld, B. A. Brown, T. Glasmacher, P. G. Hansen, R. W. Ibbotson, P. A. Lofy, V. Maddalena, K. Miller, T. Nakamura, B. V. Pritychenko, B. M. Sherrill, E. Spears, M. Steiner, J. A. Tostevin, J. Yurkon, and A. Wagner, Phys. Rev. Lett. **85**, 266 (2000).

[12] S. D. Pain, W. N. Catford, N. A. Orr, J. C. Angélique, N. I. Ashwood, V. Bouchat, N. M. Clarke, N. Curtis, M. Freer, B. R. Fulton, F. Hanappe, M. Labiche, J. L. Lecouey, R. C. Lemmon, D. Mahboub, A. Ninane, G. Normand, N. Soić, L. Stuttge, C. N. Timis, J. A. Tostevin, J. S. Winfield, and V. Ziman, Phys. Rev. Lett. **96**, 032502 (2006).

[13] R. Meharchand, R. G. T. Zegers, B. A. Brown, S. M. Austin, T. Baugher, D. Bazin, J. Deaven, A. Gade, G. F. Grinyer, C. J. Guess, M. E. Howard, H. Iwasaki, S. McDaniel, K. Meierbachtol, G. Perdikakis, J. Pereira, A. M. Prinke, A. Ratkiewicz, A. Signoracci, S. Stroberg, L. Valdez, P. Voss, K. A. Walsh, D. Weisshaar, and R. Winkler, Phys. Rev. Lett. **108**, 122501 (2012).

[14] F. C. Barker, J. Phys. G: Nucl. Part. Phys. **2**, L45 (1976).

[15] H. T. Fortune and R. Sherr, Phys. Rev. C **74**, 024301 (2006).

[16] N. C. Summers and F. M. Nunes, Phys. Rev. C **76**, 014611 (2007).

[17] C. Romero-Redondo, E. Garrido, D. V. Fedorov, and A. S. Jensen, Phys. Rev. C **77**, 054313 (2008).

[18] G. Gori, F. Barranco, E. Vigezzi, and R. A. Broglia, Phys. Rev. C **69**, 041302 (2004).

[19] G. Blanchon, N. V. Mau, A. Bonaccorso, M. Dupuis, and N. Pillet, Phys. Rev. C **82**, 034313 (2010).

[20] R. Sherr and H. T. Fortune, Phys. Rev. C **60**, 064323 (1999).

[21] F. C. Barker, J. Phys. **G36**, 038001 (2009).

[22] R. Kanungo, A. Gallant, M. Uchida, C. Andreoiu, R. Austin, D. Bandyopadhyay, G. Ball, J. Becker, A. Boston, H. Boston, B. Brown, L. Buchmann, S. Colosimo, R. Clark, D. Cline, D. Cross, H. Dare, B. Davids, T. Drake, M. Djongolov, P. Finlay, N. Galinski, P. Garrett, A. Garnsworthy, K. Green, S. Grist, G. Hackman, L. Harkness, A. Hayes, D. Howell, A. Hurst, H. Jeppesen, K. Leach, A. Macchiavelli, D. Oxley, C. Pearson, B. Pietras, A. Phillips, S. Rigby, C. Ruiz, G. Ruprecht, F. Sarazin, M. Schumaker, A. Shotter, C. Sumitharachchi, C. Svensson, I. Tanihata, S. Triambak, C. Unsworth, S. Williams, P. Walden, J. Wong, and C. Wu, Phys. Lett. B **682**, 391 (2010).

[23] D. Santiago-Gonzalez, K. Auranen, M. L. Avila, A. D. Ayangeakaa, B. B. Back, S. Bottoni, M. P. Carpenter, J. Chen, C. M. Deibel, A. A. Hood, C. R. Hoffman, R. V. F. Janssens, C. L. Jiang, B. P. Kay, S. A. Kuvin, A. Lauer, J. P. Schiffer, J. Sethi, R. Talwar, I. Wiedenhöver, J. Winkelbauer, and S. Zhu, Phys. Rev. Lett. **120**, 122503 (2018).

[24] C. R. Hoffman, B. B. Back, B. P. Kay, J. P. Schiffer, M. Alcorta, S. I. Baker, S. Bedoor, P. F. Bertone, J. A. Clark, C. M. Deibel, B. DiGiovine, S. J. Freeman, J. P. Greene, J. C. Lighthall, S. T. Marley, R. C. Pardo, K. E. Rehm, A. Rojas, D. Santiago-Gonzalez, D. K. Sharp, D. V. Shetty, J. S. Thomas, I. Wiedenhöver, and A. H. Wuosmaa, Phys. Rev. C **85**, 054318 (2012).

[25] C. R. Hoffman, M. Albers, M. Alcorta, S. Almaraz-Calderon, B. B. Back, S. I. Baker, S. Bedoor, P. F. Bertone, B. P. Kay, J. C. Lighthall, T. Palchan, R. C. Pardo, G. Perdikakis, K. E. Rehm, A. M. Rogers, D. Santiago-Gonzalez, C. Yuan, and J. P. Schiffer, Phys. Rev. C **88**, 044317 (2013).

[26] J. G. Johansen, V. Bildstein, M. J. G. Borge, M. Cubero, J. Diriken, J. Elseviers, L. M. Fraile, H. O. U. Fynbo, L. P. Gaffney, R. Gernhäuser, B. Jonson, G. T. Koldste, J. Konki, T. Kröll, R. Krücken, D. Mücher, T. Nilsson, K. Nowak, J. Pakarinen, V. Pesudo, R. Raabe, K. Riisager, M. Seidlitz, O. Tengblad, H. Törnqvist, D. Voulot, N. Warr, F. Wenander, K. Wimmer, and H. De Witte, Phys. Rev. C **88**, 044619 (2013).

[27] J. Chen, J. Lou, Y. Ye, Z. Li, D. Pang, C. Yuan, Y. Ge, Q. Li, H. Hua, D. Jiang, X. Yang, F. Xu, J. Pei, J. Li, W. Jiang, Y. Sun, H. Zang, Y. Zhang, N. Aoi, E. Ideguchi, H. Ong, J. Lee, J. Wu, H. Liu, C. Wen, Y. Ayyad, K. Hatanaka, D. Tran, T. Yamamoto, M. Tanaka, and T. Suzuki, Phys. Lett. B **781**, 412 (2018).

[28] T. Shimoda, H. Miyatake, and S. Morinobu, Nucl. Inst. Meth. Phys. Res. B **70** (1992).

[29] J. Chen, J. L. Lou, Y. L. Ye, Z. H. Li, Y. C. Ge, Q. T. Li, J. Li, W. Jiang, Y. L. Sun, H. L. Zang, N. Aoi, E. Ideguchi, H. J. Ong, Y. Ayyad, K. Hatanaka, D. T. Tran, T. Yamamoto, M. Tanaka, T. Suzuki, N. T. Tho, J. Rangel, A. M. Moro, D. Y. Pang, J. Lee, J. Wu, H. N. Liu, and C. Wen, Phys. Rev. C **93**, 034623 (2016).

[30] J. Chen, J. L. Lou, Y. L. Ye, J. Rangel, A. M. Moro, D. Y. Pang, Z. H. Li, Y. C. Ge, Q. T. Li, J. Li, W. Jiang, Y. L. Sun, H. L. Zang, Y. Zhang, N. Aoi, E. Ideguchi, H. J. Ong, J. Lee, J. Wu, H. N. Liu, C. Wen, Y. Ayyad, K. Hatanaka, T. D. Tran, T. Yamamoto, M. Tanaka, T. Suzuki, and T. T. Nguyen, Phys. Rev. C **94**, 064620 (2016).

[31] H. Baba, T. Ichihara, T. Ohnishi, S. Takeuchi, K. Yoshida, Y. Watanabe, S. Ota, and S. Shimoura, Nuclear Instruments and Methods in Physics Research Section A: Accelerators, Spectrometers, Detectors and Associated Equipment **616**, 65 (2010).

[32] M. D. Cortina-Gil, P. Roussel-Chomaz, and N. Alamanos, Phys. Lett. B **401** (1997).

[33] J. Chen, J. Lou, and D. Pang, Sci. China Phys. Mech. Astron **59**, 632003 (2016).

[34] R. Varner, W. Thompson, T. McAbee, E. Ludwig, and T. Clegg, Phys. Rep. **201**, 57 (1991).

[35] Y. Zhang, D. Y. Pang, and J. L. Lou, Phys. Rev. C **94**, 014619 (2016).

[36] P. Descouvemont, Phys. Lett. B **772**, 1 (2017).

[37] S. Shimoura, S. Ota, K. Demichi, N. Aoi, H. Baba, Z. Elekes, T. Fukuchi, T. Gomi, K. Hasegawa, E. Ideguchi, M. Ishihara, N. Iwasa, H. Iwasaki, S. Kanno, S. Kubono, K. Kurita, M. Kurokawa, Y. Matsuyama, S. Michimasa, K. Miller, T. Minemura, T. Motobayashi, T. Murakami, M. Notani, A. Odahara, A. Saito, H. Sakurai, E. Takeshita, S. Takeuchi, M. Tamaki, T. Teranishi, K. Yamada, Y. Yanagisawa, and I. Hamamoto, Phys. Lett. B **654**, 87 (2007).

[38] S. Shimoura, A. Saito, T. Minemura, Y. Matsuyama, H. Baba, H. Akiyoshi, N. Aoi, T. Gomi, Y. Higurashi, K. Ieki, N. Imai, N. Iwasa, H. Iwasaki, S. Kanno, S. Kubono, M. Kunibu, S. Michimasa, T. Motobayashi, T. Nakamura, H. Sakurai, M. Serata, E. Takeshita, S. Takeuchi, T. Teranishi, K. Ue, K. Yamada, Y. Yanagisawa, M. Ishihara, and N. Itagaki, Phys. Lett. B **560**, 31 (2003).

[39] J. L. Lou, Z. H. Li, Y. L. Ye, H. Hua, D. X. Jiang, L. H. Lv, Z. Kong, Y. M. Zhang, F. R. Xu, T. Zheng, X. Q. Li, Y. C. Ge, C. Wu, G. L. Zhang, Z. Q. Chen, C. Li, D. Y. Pang, H. S. Xu, Z. Y. Sun, L. M. Duan, Z. G. Hu, R. J. Hu, H. G. Xu, R. S. Mao, Y. Wang, X. H. Yuan, H. Gao, L. J. Wu, H. R. Qi, T. H. Huang, F. Fu, F. Jia, Q. Gao, X. L. Ding, J. L. Han, and X. Y. Zhang, Phys. Rev. C **75**, 057302 (2007).

[40] Z. H. Li, J. L. Lou, Y. L. Ye, H. Hua, D. X. Jiang, X. Q. Li, S. Q. Zhang, T. Zheng, Y. C. Ge, Z. Kong, L. H. Lv, C. Li, F. Lu, F. Y. Fan, Z. Y. Li, Z. X. Cao, L. Y. Ma, Q. Faisal, H. S. Xu, Z. G. Hu, M. Wang, X. G. Lei, L. M. Duan, Z. G. Xiao, W. L. Zhan, G. Q. Xiao, T. H. Huang, F. Fu, X. H. Zhang, C. Zheng, Y. H. Yu, X. L. Tu, Y. P. Zhang, Y. Y. Yang, H. B. Zhang, B. Thang, Y. L. Tian, Z. Ouang, M. R. Huang, Z. G. Xu, K. Yue, and Q. Gao, Phys. Rev. C **80**, 054315 (2009).

[41] E. S. Paul, P. J. Woods, T. Davinson, R. D. Page, P. J. Sellin, C. W. Beausang, R. M. Clark, R. A. Cunningham, S. A. Forbes, D. B. Fossan, A. Gizon, J. Gizon, K. Hauschild, I. M. Hibbert, A. N. James, D. R. LaFosse, I. Lazarus, H. Schnare, J. Simpson, R. Wadsworth, and M. P. Waring, Phys. Rev. C **51**, 78 (1995).

[42] S. Agostinelli, J. Allison, and K. Amako, Nucl. Instr. and Meth. Phys. Res. A **506**, 250 (2003).

[43] I. J. Thompson, Comp. Phys. Rep. **7**, 167 (1988).

[44] R. V. Reid, Ann. Phys. **50**, 411 (1968).

[45] A. Korsheninnikov, K. Yoshida, D. Aleksandrov, N. Aoi, Y. Doki, N. Inabe, M. Fujimaki, T. Kobayashi, H. Kumagai, C.-B. Moon, E. Nikolskii, M. Obuti, A. Ogloblin, A. Ozawa, S. Shimoura, T. Suzuki, I. Tanihata, Y. Watanabe, and M. Yanokura, Phys. Lett. B **316**, 38 (1993).

[46] B. P. Kay, J. P. Schiffer, and S. J. Freeman, Phys. Rev. Lett. **111**, 042502 (2013).

[47] V. R. Pandharipande, I. Sick, and P. K. A. d. Huberts, Rev. Mod. Phys. **69**, 981 (1997).

[48] J. P. Schiffer, C. R. Hoffman, B. P. Kay, J. A. Clark, C. M. Deibel, S. J. Freeman, A. M. Howard, A. J. Mitchell, P. D. Parker, D. K. Sharp, and J. S. Thomas, Phys. Rev. Lett. **108**, 022501 (2012).

[49] M. H. Macfarlane and J. B. French, Rev. Mod. Phys. **32**, 567 (1960).

[50] J. K. Smith, T. Baumann, D. Bazin, J. Brown, S. Casarotto, P. A. DeYoung, N. Frank, J. Hinnefeld, M. Hoffman, M. D. Jones, Z. Kohley, B. Luther, B. Marks, N. Smith, J. Snyder, A. Spyrou, S. L. Stephenson, M. Thoennessen, N. Viscariello, and S. J. Williams, Phys. Rev. C **90**, 024309 (2014).

[51] C. Yuan, T. Suzuki, T. Otsuka, F. Xu, and N. Tsunoda, Phys. Rev. C **85**, 064324 (2012).

[52] C.-X. Yuan, Chin. Phys. C **41**, 104102 (2017).

[53] "National nuclear data center," `http://www.nndc.bnl.gov/`.

[54] D. J. Millener, J. W. Olness, E. K. Warburton, and S. S. Hanna, Phys. Rev. C **28**, 497 (1983).

[55] L. X. Chung, C. A. Bertulani, P. Egelhof, S. Ilieva, D. T. Khoa, and O. A. Kiselev, Phys. Lett. B **774**, 559 (2017).

[56] I. Tanihata, H. Savajols, and R. Kanungo, Prog. Part. and Nucl. Phys. **68**, 215 (2013).

[57] N. Ashwood, M. Freer, S. Ahmed, J. Angelique, V. Bouchat, W. Catford, N. Clarke, N. Curtis, O. Dorvaux, B. Fulton, F. Hanappe, Y. Kerckx, M. Labiche, J. Lecouey, R. Lemmon, F. Marques, T. Materna, A. Ninane, G. Normand, N. Orr, S. Pain, N. Soic, L. Stuttge, C. Timis, A. Unshakova, J. Winfield, and V. Ziman, Phys. Lett. B **580**, 129 (2004).

[58] Z. H. Yang, Y. L. Ye, Z. H. Li, J. L. Lou, J. S. Wang, D. X. Jiang, Y. C. Ge, Q. T. Li, H. Hua, X. Q. Li, F. R. Xu, J. C. Pei, R. Qiao, H. B. You, H. Wang, Z. Y. Tian, K. A. Li, Y. L. Sun, H. N. Liu, J. Chen, J. Wu, J. Li, W. Jiang, C. Wen, B. Yang, Y. Y. Yang, P. Ma, J. B. Ma, S. L. Jin, J. L. Han, and J. Lee, Phys. Rev. Lett. **112**, 162501 (2014).

[59] W. Jiang, Y. Ye, Z. Li, C. Lin, Q. Li, Y. Ge, J. Lou, D. Jiang, J. Li, Z. Tian, J. Feng, B. Yang, Z. Yang, J. Chen, H. Zang, Q. Liu, P. Li, Z. Chen, Y. Zhang, Y. Liu, X. Sun, J. Ma, H. Jia, X. Xu, L. Yang, N. Ma, and L. Sun, Sci. China-Phys. Mech. Astron. **60**, 062011 (2017).

[60] Z. Yang, Y. Ye, Z. Li, J. Lou, F. Xu, J. Pei, Z. Tian, K. Li, Y. Sun, J. Chen, J. Li, W. Jiang, B. Yang, S. Chen, Q. Liu, H. Zang, J. Feng, and Z. Yin, Sci. China-Phys. Mech. Astron. **57**, 1613 (2014).

[61] Z. H. Yang, Y. L. Ye, Z. H. Li, J. L. Lou, J. S. Wang, D. X. Jiang, Y. C. Ge, Q. T. Li, H. Hua, X. Q. Li, F. R. Xu, J. C. Pei, R. Qiao, H. B. You, H. Wang, Z. Y. Tian, K. A. Li, Y. L. Sun, H. N. Liu, J. Chen, J. Wu, J. Li, W. Jiang, C. Wen, B. Yang, Y. Liu, Y. Y. Yang, P. Ma, J. B. Ma, S. L. Jin, J. L. Han, and J. Lee, Phys. Rev. C **91**, 024304 (2015).